

## SYNTHESIS OF INDIUM PHOSPHIDE / ZINC PHOSPHATE CORE-SHELL NANOWIRES

A. JISHIASHVILI<sup>a</sup>, Z. SHIOLASHVILI<sup>a</sup>, N. MAKHATADZE<sup>a</sup>,  
D. JISHIASHVILI<sup>a,b</sup>, D. KANCHAVELI<sup>a</sup>, D. SUKHANOV<sup>a</sup>

<sup>a</sup>Department of Physics, Georgian Technical University, 77 Kostava St., 0160,  
Tbilisi, Georgia

<sup>b</sup>E. Andronikashvili Institute of Physics, I. Javakishvili Tbilisi State University, 6  
M. Tamarashvili St., 0177, Tbilisi, Georgia

Zn<sub>3</sub>(PO<sub>4</sub>)<sub>2</sub>/InP core-shell nanowires were grown by a one-step pyrolytic synthesis in a vapor of hydrazine containing 3mol.% H<sub>2</sub>O. InP+Zn and InP+ZnO were used as sources for producing volatile species that were forming nanowires in the cold zone of a reactor. The cores were crystalline InP, while the zinc phosphate shells had amorphous structure because the growth temperature (500°C) was insufficient for their crystallization. The most favorable thermochemical reactions that may produce core and shell materials were evaluated. It was established that the amorphous Zn<sub>3</sub>(PO<sub>4</sub>)<sub>2</sub> shell was growing by a template-based Vapor-Solid method. InP core and ring-shaped Zn<sub>3</sub>(PO<sub>4</sub>)<sub>2</sub> shell, formed at the initial stage of synthesis, served as templates for the growth of shell. The nanotubes of zinc phosphate were produced at 540°C, when the source contained a low amount of InP. This happened because the template-based growth of a shell proceeded even after the growth of InP core was stopped.

(Received February 10, 2018; Accepted June 5, 2018)

*Keywords:* Zinc phosphate, Core-shell, nanowire, InP, Hydrazine, Amorphous nanostructure

### 1. Introduction

One-dimensional nanomaterials, particularly core-shell nanowires attracted a great interest due to substantial potential for their application in advanced nanodevices [1-3]. In contrast to ordinary nanowires, the properties of core-shell nanostructures can be tailored by selecting proper shell material or by processes that take place at the core-shell interface [4-7].

Zinc phosphate is an interesting material to be used as the shell in core-shell nanostructures. In addition to some important fields of applications [8,9], it is of particular interest for biomedical usage because Zn<sub>3</sub>(PO<sub>4</sub>)<sub>2</sub> has long been proven to be a non-toxic material, which is used as a basis for dental cement since 19<sup>th</sup> century [8]. One of the interesting features that was found when investigating Zn<sub>3</sub>(PO<sub>4</sub>)<sub>2</sub>-based nanomaterials was their ability to self assemble in the presence of templates like viruses, proteins, microalgae etc. [10-13]. The important topic of modern nanotechnology is the growth of amorphous nanomaterials, which offers new possibilities for the fabrication of high-quality multifunctional nanostructures. Though some amorphous zinc phosphate nanomaterials have been already synthesized [14-16], this technological issue is still at the beginning stage of development and our paper addresses exactly this subject.

The purpose of this work was to synthesize the core-shell nanowires comprising the crystalline InP core and the amorphous Zn<sub>3</sub>(PO<sub>4</sub>)<sub>2</sub> shell, and to study their composition, structure and growth mechanism.

---

\*Corresponding author: d\_jishiashvili@gtu.ge

## 2. Experimental

In our previous works we have developed the hydrazine-based pyrolytic technology for the growth of different nanowires [17]. Briefly, this technology implies the annealing of InP+Zn or InP+ZnO solid sources, placed on the bottom of a vertical quartz reactor, in hydrazine ( $N_2H_4$ ) vapor diluted with 3 mol.% water. The formation of volatile precursors and chemical reactions that take place on Si substrate will be considered in the next section.

The morphology and structure of NWs were studied using Tescan Vega 3 LMU Scanning Electron Microscope (SEM) and Philips CM200 FEG Transmission Electron Microscope (TEM). Fourier-transform IR spectra were taken on Shimadzu IRAffinity-1S Spectrophotometer.

## 3. Results and discussion

For the growth of nanowires InP+Zn or InP+ZnO source was placed on the bottom of a vertical quartz reactor and annealed up to  $750^\circ C$  in hydrazine vapor with a pressure of  $\sim 10$  Torr. The Si substrate was located 2 cm above the source and heated up to  $550^\circ C$ . The gaseous precursors that were produced after dissociation of InP and interaction of sources with hydrazine pyrolytic decomposition products, were reaching the Si substrate and reacting with each other forming the nanowires.

The phosphorous vapor was provided by dissociation of InP source at elevated temperatures. It has been reported that the atomic hydrogen, which in our technology can be generated via hydrazine decomposition, may reduce the InP decomposition temperature by  $230^\circ C$ , thereby promoting the formation of P,  $P_2$ ,  $P_4$  and  $PH_3$  species with a pressure up to  $10^{-5}$  Torr [18,19]. Besides phosphorus, the decomposition of InP caused the appearance of In droplets, which formed the volatile  $In_2O$  molecules after interacting with water vapor [17].

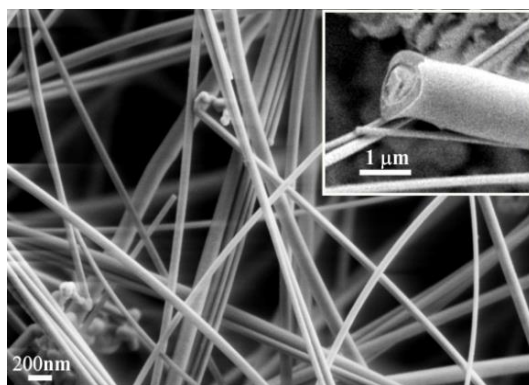


*Fig. 1. SEM image of nanowires grown from InP+Zn Source. Inset shows the cross-sectional view of the nanowire.*

The pure Zn powder, which has a low melting point ( $420^\circ C$ ), easily sublimates and its saturated pressure is high even at low temperatures (e.g.  $10^{-4}$  Torr at  $250^\circ C$  [20]). In contrast to Zn, ZnO has a relatively higher melting point ( $1975^\circ C$ ) and dissociation temperature [21,22]. Usually, when ZnO is used as a source material, hydrogen and halogens are used to produce volatile Zn compounds and accomplish its mass transport [23-25]. When hydrogen is used, the chemistry of the process is based on the reduction of Zn from ZnO and its subsequent sublimation. However, the temperature of this process is still high, exceeding  $1000^\circ C$  [26,27] because the corresponding reaction of Zn reduction by hydrogen has a positive Gibbs free energy even at  $1000^\circ C$ . As it was shown [17], the active NH and  $NH_2$  radicals together with hydrogen (atomic and molecular) are presented in the pyrolytic decomposition products of hydrazine. These radicals helped to significantly decrease the growth temperatures of  $Ge_3N_4$  and InN nanowires in hydrazine, as

compared to the synthesis from ammonia [28]. The highest negative value of Gibbs free energy (calculated at 500°C) has the reaction of ZnO reduction by NH radicals:



This indicates that Zn will be easily produced in our technology, while the water molecules that will be synthesized by reaction (1) may promote the formation of oxides in the cold zone of the reactor or serve for producing volatile  $\text{In}_2\text{O}$  species.

The SEM image of nanowires formed from the  $\text{InP} + \text{Zn}$  source on the Si substrate heated up to 440°C is presented in Fig. 1 (the source temperature was 500°C). The inset shows the cross section of a broken thick nanowire. The nanowires have uniform diameters along the growth direction and circular cross sections. Their lengths reach several micrometers and the diameters deviate in a wide range beginning from 20 nm. The absence of catalyst tips confirms that the NWs are growing by the Vapor-Solid (VS) mechanism.

The high-resolution TEM (HRTEM) image of the nanowire is presented in Fig.2. It consists of a crystalline core and an amorphous shell. The inset in Fig.2 shows the Fast Fourier Transform (FFT) of a core material. It was established that the crystalline core comprises indium phosphide with a wurtzite structure, which is growing along [0001] direction. The bulk InP has a zinc-blende (ZB) structure, while in 1D InP NWs the wurtzite (WZ) structure is frequently observed. This happens because the nanowires have the increased surface to volume ratio, which forces the growing NW to adopt the WZ structure that has a lower surface energy in comparison with ZB nanowire [29,30].

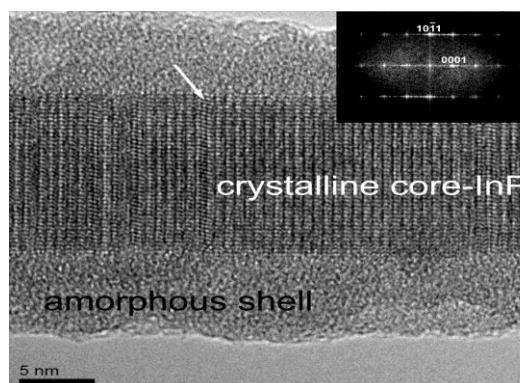


Fig.2. HRTEM view of the core-shell nanowire and corresponding FFT. Arrow indicates the stacking fault.

The polytypism is usually observed in III-V nanowires [31]. The vertical lines in HRTEM image of WZ nanowire are formed by tetrahedrally bonded In and P atomic layers that are stacked in an order, in which the bonds in the subsequent layers are rotated by 60° (the so called A and B layers). In ZB structure the bonds in the neighboring bilayers are directed in the same direction and the three layers are shifted to form the sequence ABC and then again ABC. Insertion of one Zinc-blende segment in WZ structure causes the appearance of a stacking fault as it is illustrated in Fig.2 by a white arrow. The inset in Fig.2 clearly shows the streaks in the [0001] direction, which are indicative of defects, like one considered above, that are oriented perpendicular to this axis. The average diameter of nanowire in Fig.2 was estimated to be 29 nm, while that of a crystalline InP core was 14 nm.

The composition of a shell was studied using EDS and IR spectroscopy. The results of EDS measurements are presented in the insets of Fig. 3, together with High Angle Annular Dark Field (HAADF) TEM image of two core-shell nanowires. These qualitative experiments were aimed at the detection of main chemical elements existing in the grown nanowires. The red rectangles show the areas from which the EDS signals were recorded. Two of them (a and d) are

representing the composition of shells, while b and c rectangles yield the composition of cores. The comparison of core and shell induced EDS spectra clearly shows that the In content in core is significantly higher, and that In, P, Zn and oxygen are main constituents of nanowires.

Direct information about the composition of shell material was obtained by IR spectroscopy. Fig.4 presents the IR spectrum of nanowires, which were scrapped off the Si substrate, mixed with KBr powder and pressed in a pellet. By analyzing the IR spectrum it was established that the shells are formed by the amorphous zinc phosphate  $\text{Zn}_3(\text{PO}_4)_2$  [14,16,32]. The broad absorption bands centered at  $\sim 1000$  and  $\sim 550$   $\text{cm}^{-1}$  are attributed to the complex stretching and bending vibration bands of  $\text{PO}_4^{3-}$  group, which are broadened due to the amorphous structure of a shell material. The absence of bands at  $\sim 1650$  and  $\sim 3425$   $\text{cm}^{-1}$ , which are attributed to  $\text{OH}^-$  bending and stretching vibrations, shows that the  $\text{Zn}_3(\text{PO}_4)_2$  shell is not hydrated [33,34].

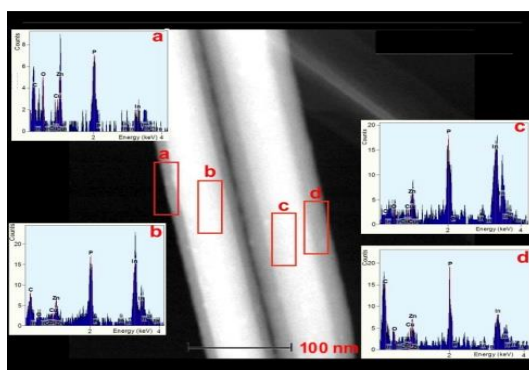


Fig.3. HAADF TEM image of two nanowires grown from InP+Zn source. Insets from a to d are EDS spectra recorded from the corresponding rectangles depicted in the TEM image.

The results of these experiments clearly showed that when In+Zn was used, the core-shell nanowires were produced with crystalline InP core and an amorphous  $\text{Zn}_3(\text{PO}_4)_2$  shell. Substitution of Zn with ZnO in a source doesn't alter the structure and composition of nanowires. However, the thickness of a shell increases.

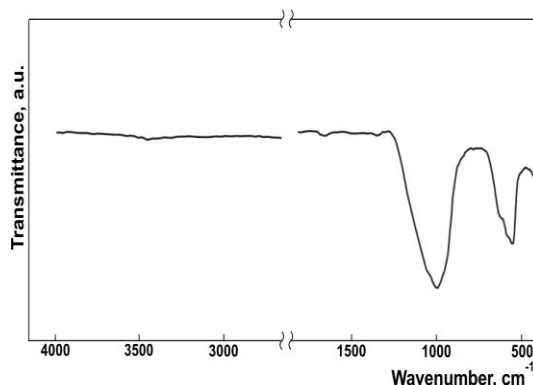


Fig.4. IR spectra of core-shell nanowires produced from InP+Zn source.

Fig.5 shows the TEM image of nanowire synthesized at 500°C using InP+ZnO source. As can be seen, the shell thickness has been increased in comparison with nanowire grown from InP+Zn source (Fig. 2). The nanowire cores in Fig.5 and Fig. 2 have the same diameters ( $\sim 14$  nm), while the shell thickness is by 2.8 times larger in the case when ZnO source was used. Such increase of a shell thickness can be attributed to the effectiveness of ZnO reduction reactions in hydrazine vapor. Beside Zn, these reactions are producing water molecules, thus enhancing the

yield of oxygen-containing  $\text{Zn}_3(\text{PO}_4)_2$  material and increasing the thickness of a shell. Our preliminary results indicated that the thickness of  $\text{Zn}_3(\text{PO}_4)_2$  shell can be regulated by adding controlled amounts of ZnO powder to the Zn+InP source.

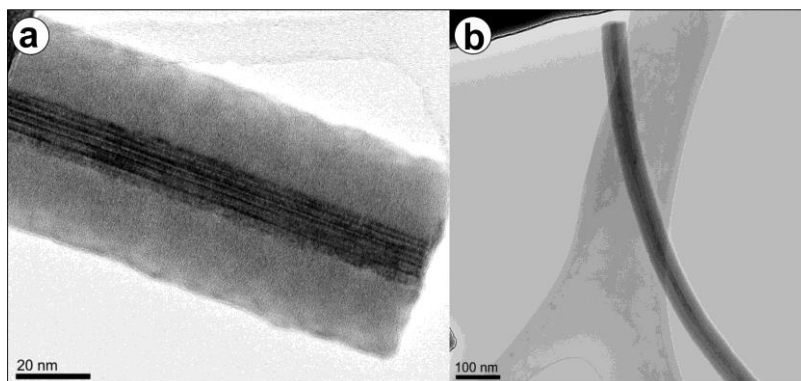
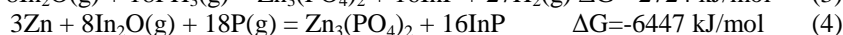
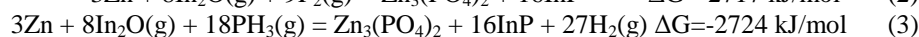
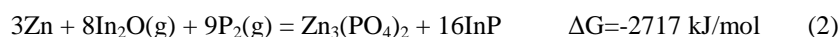


Fig. 5. HRTEM (a) and TEM images (b) of  $\text{Zn}_3(\text{PO}_4)_2/\text{InP}$  NWs grown from InP+ZnO source.

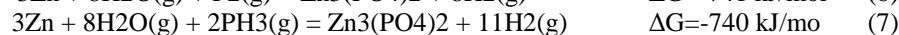
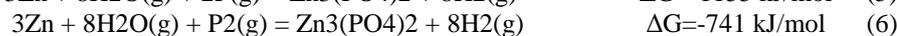
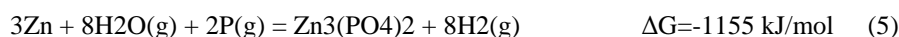
The formation of core-shell nanowires in hydrazine-based pyrolytic technology proceeds as a one-step process. The crystalline InP core and the amorphous shell are produced simultaneously, most likely due to spontaneous segregation of phases. A necessary and sufficient condition for a spontaneous process to proceed is the negative sign of Gibbs free energy and a high value of a kinetic factor of the corresponding thermochemical reaction.

We have estimated the Gibbs free energy values and signs for possible chemical reactions, which may take place between gaseous precursors existing in our reactor (Zn,  $\text{In}_2\text{O}$ ,  $\text{H}_2\text{O}$ ,  $\text{O}_2$ ,  $\text{H}_2$ , H, P,  $\text{P}_2$ ,  $\text{P}_4$ ,  $\text{PH}_3$ ). The analysis showed that  $\text{Zn}_3(\text{PO}_4)_2$  and InP can be formed separately or together by different thermodynamically favorable chemical reactions. However, the reactions, in which  $\text{Zn}_3(\text{PO}_4)_2$  and InP phases are spontaneously synthesized and segregated have the highest negative values of a Gibbs free energy:



The analysis of  $\text{Zn}_3(\text{PO}_4)_2$  shell formation deserves special attention. If the shells were produced only by segregation reactions (2), (3) and (4), then for NWs with equal core diameters grown from both sources, the shell thicknesses should be also equal. This, however, is not the case, indicating that there exists some other source of  $\text{Zn}_3(\text{PO}_4)_2$ , which affects the shell thickness. Besides, according to reactions (2), (3) and (4), in the absence of re-evaporation the amount of produced InP should greatly exceed that of  $\text{Zn}_3(\text{PO}_4)_2$ . However, the thicknesses of shells in Fig.2 and Fig. 5 are larger, than the diameter of InP core, indicating once again that there exist an additional source of  $\text{Zn}_3(\text{PO}_4)_2$ .

As noted above, in our technology there are several thermodynamically favorable reactions that may produce  $\text{Zn}_3(\text{PO}_4)_2$ . Three of these reactions with high negative Gibbs energies are listed below:



The formation of zinc phosphate molecules at the growing nanowire surfaces may cause a sidewall deposition. This will result in the growth of tapered nanowires with thicker shells near the bottoms and thinner near the growth fronts. However, this mechanism should be eliminated

because the nanowires have uniform diameters along the growth direction, as it is shown in Fig. 5a,b.

The possible mechanism of a shell formation can be understood by analyzing the nanowires grown at elevated temperatures using InP deficient source. Fig. 6 shows SEM images of nanostructures grown at 540°C from InP+Zn source with a low InP content (the weight ratio InP/Zn=0.6). The tubes with diameters of approximately 600 nm are clearly seen, which appear on the background of different byproducts formed on the Si substrate. Some of the tubes are still filled with InP, but the tips of most of them are hollow. The deficiency of indium resulted in a rapid depletion of a source and at a certain point when Indium supply was stopped the growth of InP core become impossible. At the same time, the precursors that were needed for the synthesis of  $Zn_3(PO_4)_2$  shell (phosphorus, Zn and  $H_2O$ ) were still presented in the reactor. The cross section of a ring-shaped  $Zn_3(PO_4)_2$  shell, which was surrounding the crystalline InP core, served as a hard template for the growth of tubular  $Zn_3(PO_4)_2$  nanomaterials. Such template-based growth methods are widely used for producing crystalline and amorphous nanomaterials [15,35-37].

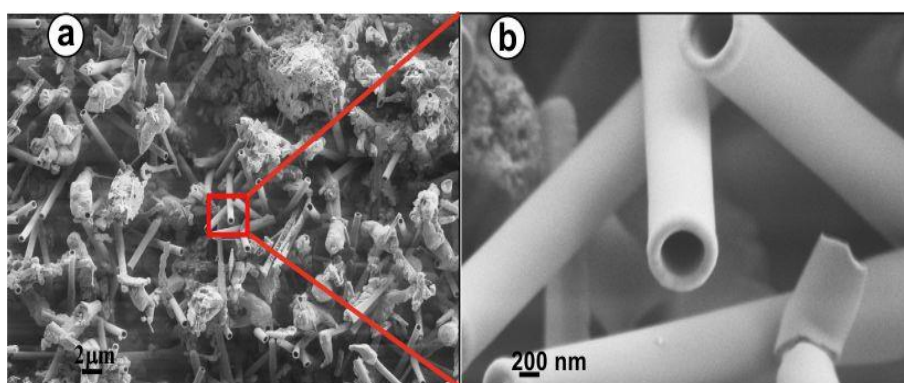


Fig.6. Low (a), and high magnification (b) SEM images of nanotubes, grown at the deficiency of InP in InP+Zn source. The growth temperature was 540 °C.

The anisotropy of properties and the lack of long-range order eliminates the possibility for amorphous materials to grow as 1D nanostructures, except the cases, when template-based methods or special guiding techniques are used [15]. These methods exclude the lateral growth of nanowires, forcing the growing amorphous material to form the template-like elongated nanomaterials.

The obtained results indicate that only a small part of the amorphous  $Zn_3(PO_4)_2$  shell may originate due to the segregation reactions (2), (3) and (4). These reactions can be important for the formation of the first core-shell seeds and solid templates at the initial stage of nanowire growth. After that, the predominant amount of a shell material will be produced by direct template-based synthesis from existing precursors.

The core-shell nanowires may be produced even without segregation reactions. The growing InP nanowire side wall itself may serve as a substrate for the formation of an initial ring-shaped  $Zn_3(PO_4)_2$  shell, which then will be used as a solid template for the growth of a tubular nanostructure around the core. Such growth mechanisms of amorphous 1D nanostructures were considered in [15].

It should be noted, that the formation of tubular zinc phosphates in our experiments may be caused also by an increased growth rate of  $Zn_3(PO_4)_2$  shell, which can exceed the growth rate of InP crystalline core at elevated temperatures. However, our observations showed that the zinc phosphate tubes were formed only in cases when the indium deficient sources were used, thus excluding the growth rate related factors.

As discussed previously, the pressures of Zn and phosphorus are considered to be sufficiently high. The main limiting factor for direct synthesis of zinc phosphate is the concentration of  $H_2O$ , which increases when using ZnO source due to reactions (1) and similar

reduction reactions. Accordingly, the thickness of an amorphous zinc phosphate shell increases for nanowires grown from InP+ZnO source, as it is observed in Fig. 5.

Nanoscale amorphous materials are very important members of the non-crystalline solids family and have emerged as a new category of advanced materials [15]. However, morphological control of amorphous nanomaterials is very difficult because of the atomic isotropy of their internal structures [15,37]. The growth of amorphous zinc phosphate nanotubes and  $\text{Zn}_3(\text{PO}_4)_2/\text{InP}$  core-shell nanostructures are interesting achievements in their own right, especially since the zinc phosphate shell is a corrosion-inhibiting, biocompatible, non-toxic material, which offers wide nanotechnological applications.

#### 4. Conclusions

The one-step pyrolytic technology was developed for the fabrication of core-shell nanowires comprising the crystalline InP core and the amorphous  $\text{Zn}_3(\text{PO}_4)_2$  shell. The technology implies annealing of InP+Zn or InP+ZnO sources in hydrazine containing 3 mol.%  $\text{H}_2\text{O}$  with subsequent evaporation of volatile species, which are then producing nanowires on the Si surface placed 2 cm above the sources and heated up to  $500^\circ\text{C}$ . When ZnO source was used, it was first reduced to Zn by hydrazine decomposition products and then sublimated. The reduction of ZnO caused the increase of oxygen content in the reactor. As a result, the shell thickness was also increased by 2.8 times as compared to shells synthesized from a pure Zn source.

It was established that for nanowires grown at identical process parameters, the amorphous shell thickness is larger for core-shell nanostructures produced from InP+ZnO source. Analysis of thermochemical reactions revealed that there exist a number of thermodynamically favorable chemical reactions, which may produce InP and  $\text{Zn}_3(\text{PO}_4)_2$ . However, the highest negative Gibbs energies have reactions that lead to the spontaneous segregation of InP and  $\text{Zn}_3(\text{PO}_4)_2$  phases. Even so, these segregation reactions alone cannot explain the observed large thicknesses of amorphous shells and their thickness variation with ZnO content in the source. The growth of nanowires at elevated temperatures ( $540^\circ\text{C}$ ) from indium deficient source showed that the most of amorphous  $\text{Zn}_3(\text{PO}_4)_2$  was produced by direct synthesis on the surface of ring-shaped zinc phosphate template, which was formed around the InP crystalline core at the initial stage of nanowire growth (the so-called "template-based growth"). Even when the growth of a core stops due to the depletion of indium in the source, the shell continues to grow, preserving its tubular shape and forming  $\text{Zn}_3(\text{PO}_4)_2$  nanotubes.

#### Acknowledgements

This work was financially supported by the Shota Rustaveli National Science Foundation Grant PhDF2016\_113.

#### References

- [1] Y. Zhang, J. Wu, M.N. Aagesen, H. Liu, *Journal of Physics D: Applied Physics* **48**, 463001 (2015).
- [2] M. Fang, N. Han, F. Wang, Z. Yang, S. Yip, G. Dong, J. J. Hou, Y. Chueh, J. C. Ho, *Journal of Nanomaterials* **2014**, 1 (2014).
- [3] A. Zhang, G. Zheng, C. M. Lieber, Springer, Switzerland, 321 (2016).
- [4] M. Royo, M. De Luca, R. Rurali, I. Zardo, *Journal of Physics D: Applied Physics* **50**(14), 143001 (2017).
- [5] X. Xia, J. Tu, Y. Zhang, X. Wang, C. Gu, Z.B. Zhao, H.J. Fan, *ACS Nano* **6**(6), 5531 (2012).
- [6] Y. Dong, B. Tian, T. J. Kempa, C. M. Lieber, *Nano Letters* **9**(5), 2183 (2009).
- [7] Ch. Li, J. B. Wright, Sh. Liu, P. Lu, J. J. Figiel, B. Leung, W. W. Chow, I. Brener, D. D.

- Koleske, T. Luk, D.F. Feezell, S. R. J. Brueck, G. T. Wang, *Nano Letters* **17**(2), 1049 (2017).
- [8] A.S. Wagh, "Chemically Bonded Phosphate Ceramics: Twenty-First Century Materials with Diverse Applications", Elsevier, Amsterdam, Netherlands, 422 (2016).
- [9] A.J. Jadhav, S.E. Karekar, D.V. Pinjari, Y.G. Datar, B.A. Bhanvase, S.H. Sonawane, A. B. Pandit, *Hybrid Materials* **2**, 1 (2015).
- [10] K. Kumar, V. Penugurti, G. Levi, Y. Mastai, B. Manavathi, P. Paik, *Biomeical. Materials* **13**, 015013 (2017).
- [11] Y. Song, H. Ji, M. Wang, L. He, R. Song, *Applied Surface Science* **422**, 228 (2017).
- [12] J. Liang, L. Li, *Materials Letters* **65**, 285 (2011).
- [13] G. Santomauro, V. Srot, B. Bussmann, P. A. van Aken, F. Brümmer, H. Strunk, J. Bill, *Journal of Biomaterials and Nanobiotechnology* **3**, 362 (2012).
- [14] S. Bach, V.R. Celinski, M. Dietzsch, M. Panthöfer, R. Bienert, F. Emmerling, J. Schmedt auf der Günne, W. Tremel, *Journal of American Chemical Society* **137**, 2285 (2015).
- [15] J. Nai, J. Kang, L. Guo, *Science China Materials* **58**, 44 (2015).
- [16] S.H. Jung, E. Oh, D. Shim, D.H. Park, S. Cho, B.R. Lee, Y.U. Jeong, K.H. Lee, S.H. Jeong, *Bulletin of Korean Chemical Society* **30**, 2280 (2009).
- [17] A. Jishiashvili, Z. Shiolashvili, N. Malhatadze, D. Jishiashvili, A. Chirakadze, D. Sukhanov, D. Kanchaveli, *Oriental Journal of Chemistry* **33**, 1103 (2017).
- [18] V.I. Gorbenko, A.N. Gorban, *Radiophysics* **1**, 7 (2012).
- [19] V. I. Gorbenko, J. A. Shvets, A. N. Gorban. III-Nitride Based Semiconductor Electronics and Optical Devices and Thirty-Fourth State-of-the-Art Program on Compound Semiconductors (SOTAPOCS XXXIV): proceedings of the international symposia. Electrochemical Society Pennington, N.J. 318 (2001).
- [20] A. M. Klimova, V. A. Ananichev, M. Arif, L. N. Blinov, *Glass Physics and Chemistry* **31**, 760 (2005).
- [21] L. O. Schunk, A. Steinfeld, *AIChE Journa*, **55**, 1497 (2009).
- [22] M. Chambon, S. Abanades, G. Flamant, *AIChE Journal* **57**, 2264 (2011).
- [23] G.V. Colibaba, *Materials Science in Semiconductor Processing* **43**, 75 (2016).
- [24] J. Wang, M. Isshiki, "Wide-Bandgap II–VI Semiconductors: Growth and Properties". In: Kasap S., Capper P. (eds) "Springer Handbook of Electronic and Photonic Materials. Springer", Springer, Boston, MA, 1536 (2006).
- [25] G.V. Colibaba, *Solid State Science* **56**, 1(2016).
- [26] D.F. Anthrop, A.W. Searcy, *The Journal of Physical Chemistry* **68**, 2335 (1964).
- [27] J.-M. Ntep, M. Barbé, G. Cohen-Solal, F. Bailly, A. Lusson, R. Triboulet, *Journal of Crystal Growth* **184-185**, 1026 (1998).
- [28] D. Jishiashvili, Z. Shiolashvili, A. Chirakadze, N. Makhataadze, A. Jishiashvili, K. Gorgadze, *AIMS Materials Science* **3**, 470 (2016).
- [29] R.E. Algra, M.A. Verheijen, M.T. Borgström, L.-F. Feiner, G. Immink, W.J.P. van Enckevort, E. Vlieg, E.P.A.M. Bakkers, *Nature* **456**, 369 (2008).
- [30] M. Moewe, L. C. Chuang, V.G. Dubrovskii, C. Chang-Hasnain, *Journal of Applied Physics* **104**, 044313 (2008).
- [31] P. Caroff, J. Bollinsson, J. Johansson, *IEEE Journal of Selected Topics in Quantum Electronics* **17**, 829 (2011).
- [32] R.L. Frost, *Spectrochimica Acta Part A* **60**, 1439 (2004).
- [33] X. Zhou, H. Du, H. Ma, L. Sun, R. Cao, H. J. Li, *Journal of Physics and Chemistry of Solids* **78**, 1 (2015).
- [34] Z. L. Ning, W. J. Li, Ch. Y. Sun, P. Che, Zh. D. Chang, *Transactions of Nonferrous Metals Society of China* **23**, 718 (2013).
- [35] A. Huczko, *Applied Physics A* **70**, 365 (2000).
- [36] Y. Xie, D. Kocaeffe, C. Chen, Y. Kocaeffe, *Journal of Nanomaterials* **2016**, 2302595 (2016).
- [37] L. B. Mao, L. Xue, D. Gebauer, L. Liu, X.F. Yu, Y.Y. Liu, H. Colfen, S. H. Yu, *Nano Research* **9**, 1334 (2016).